sustainability

MDPI

Article

Configurations of Aromatic Networks for Power Distribution System

K. Prakash [1,*], F. R. Islam [2,*], K. A. Mamun [3] and H. R. Pota [1]

[1] School of Engineering and Information Technology, UNSW, Canberra, ACT 2610, Australia; h.pota@adfa.edu.au

[2] School of Science and Engineering, The University of Sunshine Coast (USC), Moreton Bay, QLD 4502, Australia

[3] School of Engineering and Physics, The University of the South Pacific (USP), Suva, Fiji; kabir.mamun@usp.ac.fj

* Correspondence: krishneel.prakash@adfa.edu.au (K.P.); fislam@usc.edu.au (F.R.I.)

Received: 10 March 2020; Accepted: 20 May 2020; Published: 25 May 2020

Abstract: A distribution network is one of the main parts of a power system that distributes power to customers. While there are various types of power distribution networks, a recently introduced novel structure of an aromatic network could begin a new era in the distribution levels of power systems and designs of microgrids or smart grids. In order to minimize blackout periods during natural disasters and provide sustainable energy, improve energy efficiency and maintain stability of a distribution network, it is essential to configure/reconfigure the network topology based on its geographical location and power demand, and also important to realize its self-healing function. In this paper, a strategy for reconfiguring aromatic networks based on structures of natural aromatic molecules is explained. Various network structures are designed, and simulations have been conducted to justify the performance of each configuration. It is found that an aromatic network does not need to be fixed in a specific configuration (i.e., a DDT structure), which provides flexibility in designing networks and demonstrates that the successful use of such structures will be a perfect solution for both distribution networks and microgrid systems in providing sustainable energy to the end users.

Keywords: aromatic network; smart grid; microgrid; network configuration; power distribution network; energy efficiency and stability; self-healing; sustainable energy

1. Introduction

Extreme natural hazards such as hurricanes have led to severe damages to the existing power grid systems over the years [1–3]. A total of 16 such events were reported in 2017 alone (including the famous hurricanes Maria, Harvey and Irma), leading to over 300 billion-dollar damages [4]. The existing power system is exceptionally vulnerable to the disruptions due to such natural hazards. For instance, study [5] states that more than 80% of all long-term power outages have been caused by the extreme weather events. Hurricane Sandy in 2012 had a severe impact on the United States power grid leaving approximately eight million people without power across the 15 states [6]. Later in 2017, approximately a quarter of a million people in Texas were left without power due to hurricane Harvey [7]. According to study [8], the number of power outages and power system grid damages is expected to increase in future as the current situation of climate change has increased the frequency and intensity of extreme weather events. As a result, grid resilience is increasingly critical, providing a pressing need for power system researchers to develop a robust and resilient power grid system to minimize severe disruptions [9].

Furthermore, study [10] elaborates that the current power grids remain vulnerable and exposed to natural disasters, hence, many power system industries are focusing onto establishing effective methods

of restoring the distribution systems quickly after the damages from disasters to make the power system grid resilient rather than protecting the power grids from disasters (such as storms) directly [6]. Restoration of distribution systems that aims at restoring critical loads after fault by modifying the topological structure (reconfiguring) of the distribution network has been comprehensively reviewed in the literature.

Civanlar et al. [11,12] conducted research on reconfiguring a primary distribution feeder to reduce losses using a scheme for planning and control with a heuristic method. A look-up table-based algorithm and a Pareto-optimization-based algorithm have been used to solve the network reconfiguration issues to achieve minimum power loss and maximum reliability of the distribution system [13]. A generic algorithm technique was used in [14,15] to reconfigure a distribution network. An optimum flow pattern was obtained by solving the Kirchhoff's Voltage Law (KVL) and Kirchhoff's Current Law (KCL) in [16], reconfigurations have been used to reduce resistive line losses in [17,18], and sensitivity, optimum power flow and heuristics techniques employed to reconfigure networks in [19,20]. Simulated annealing technique-based reconfigurations of distribution networks using methods for searching for an unacceptable non-inferior solution were proposed in [21–23]. The effectiveness of a network reconfiguration with shunt capacitors was highlighted by [24]. In [25], a time-varying load for reducing distribution losses through a network reconfiguration was considered. A generic algorithm-based fuzzy multi-objective methodology and evolutionary computation techniques for solving network reconfiguration problems in radial distribution networks were presented in [26]. Models for reconfiguring a network to minimize the energy supply cost and energy loss were proposed in [27,28]. To minimize the total loss, the problem of determining the state of switching devices in distribution networks was addressed in [29].

In online reconfigurations of active distribution networks conducted in [30], the computational burden of the optimization procedure was drastically reduced by exploiting the assessment of switching actions. In [31], an algorithm for an improved multi-agent particle swarm optimization (PSO) technique for overcoming distribution network reconfiguration problems was proposed. It combined the learning, competition and cooperation mechanisms of multi-agent technology and used the von Neumann topology in a PSO algorithm. Risk-based reconfigurations of electric distribution networks considering a reward/penalty scheme with load and generation uncertainties were presented in [32], with PSO and a scenario theory for solving optimization problems and modeling risk presented. To minimize power losses, deviations of nodes' voltages and branches' current constraint violations, reconfigurations of distribution networks considering harmonic loads were performed in [33]. A new fuzzy multi-criteria decision-making algorithm and software for the reconfiguration of a distribution network considering an analysis of the power losses of sub-transmission systems was developed in [34]. While the methods discussed above solved the problems of power and energy losses due to a fault, a straightforward robust optimization method for network reconfiguration considering load uncertainties was used in [35].

At times, natural disasters damage the substations as well which limits the main grid from supplying power to the distribution system causing blackout in isolated areas. In such a scenario, the traditional approach of restoring the distribution system does not guarantee continuous power supply to the customers after natural disaster. An alternative approach has been mentioned in [36] stating that the distributed generation (DG) units managed by microgrids can help in providing support to the critical loads after major fault occurs on main grid. However, it is a very difficult task which may also take a lot of time to efficiently form microgrids from several DGs in the distribution system especially in the case of damages done by a natural disaster.

In [37,38], dichlorodiphenyltrichloroethane (DDT), a chemical compound used as a pesticide in the early 1990s, was introduced recently for power distribution system (by our research team) with its network characteristics. The aromatic network was specifically designed to overcome the power outage issues during natural disasters making the distribution system more robust and resilient. In [37], various fault scenarios were tested on the aromatic network to verify its robustness and self-healing

characteristics. However, how this aromatic structure could be configured, and reconfigured if necessary, during a fault was not explained. Hence, in this paper, a generalized method for configuring an aromatic network, which is applicable for reconfiguring various higher-order aromatic network structures, is explained. Due to the simplicity and effectiveness regarding uncertain loads of the method used in [35], this paper modifies it for the design of a generalized scheme for configuring a new aromatic network and then reconfiguring it using higher-order Aromatic structures.

The remainder of this paper is organized as follows. Section 2 describes the original aromatic network. Section 3 formulates the approach of configuring aromatic network and reconfiguring it to other various higher order network structures. Section 4 provides analytical results and discussion, and we conclude in Section 5.

2. Description of Aromatic Network

An aromatic network was designed to overcome the drawbacks of three existing power distribution networks (radial, ring and mesh) in [37] where two physical sub-structures with similar chemical structures to that of benzene are connected through a Point of Common Coupling (PCC) that form a DDT-shaped physical structure for an Aromatic distribution network, as shown in Figure 1. Each benzene structure contains six buses, each of which is associated with its two neighboring ones connected via overhead and/or underground lines.

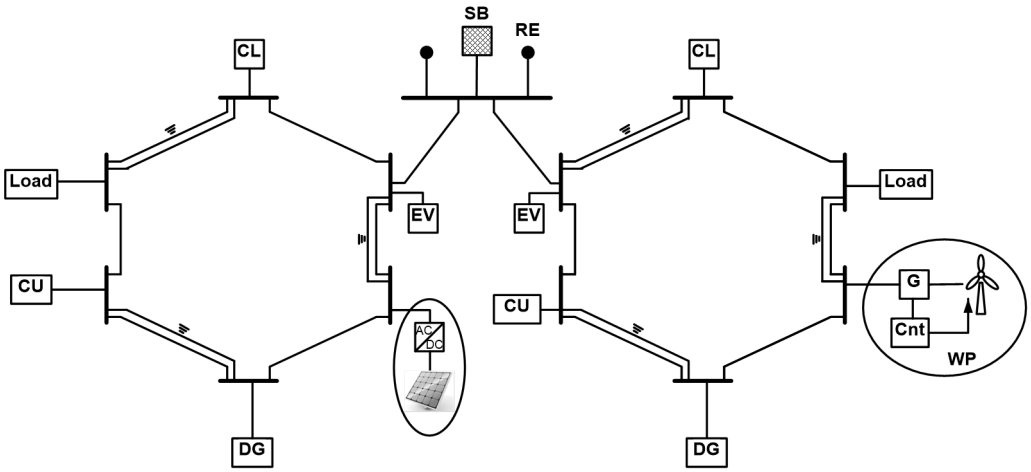

Figure 1. Aromatic network [37].

These benzene structures are synchronized through the slack bus (at the PCC) that can be connected to a synchronous generator, renewable energy source (i.e., wind, solar, hydro, etc.) or utility grid. Additional benzene structures can be connected to the PCC as, at this point; the chemical structure of DDT has more than one chlorine atom.

An aromatic network is limited to connecting only one renewable energy source per benzene structure to improve its stability while other buses can be connected with distributed generation (i.e., synchronous generators, batteries, etc.) together with their respective loads.

Each bus consists of a control system known as an 'agent' that can communicate with the nearest adjacent bus of the benzene-shaped physical structures of the Aromatic distribution network. These agents can provide information to users regarding the status of the system's voltage, frequency and other necessary parameters.

A global control system can be used at the PCC (slack bus) of an aromatic network to synchronize the two benzene structures which also provide the status of the grid (demand, generation, faults, etc.) to the national utility management system. This system contains wireless network technology for the agents to communicate and local and global control systems [39].

An aromatic network has an automatic self-healing mechanism that reconfigures its structure following any fault; for instance, if a fault occurs at a single-bond overhead transmission line, the benzene structure of an Aromatic network starts to behave like a radial network but, if a fault occurs at a double-bond lines, the overhead transmission lines are instantly substituted by the underground cables and the operation of the network remains normal. If a fault occurs between the slack bus and benzene structure or even if a fault occurs at the substation, a bus connected to a distribution generator (i.e., a diesel generator) acts as a slack bus for the benzene structure and automatically starts to operate as a micro grid. The implementation of aromatic networks will bring a new era to the power systems as it will increase the robustness and resilience of distribution system during natural disasters. A significant reduction in power outage time (blackout period) during natural disasters could be successfully achieved through an aromatic network.

3. Configuration of Basic Aromatic Network (DDT Structure)

The previous section has described the aromatic network and its importance on power system especially during natural disasters. In this section, the formulation of aromatic network configuration in DDT structure and its reconfigurations into higher-order aromatic networks based on other aromatic molecules are explained with reference to real time applications.

3.1. Aromatic Network—Configuration 1 (DDT)

An aromatic network with a DDT structure is the fundamental structure of this topology with two benzenes connected to it through the PCC, as shown in Figure 2. Each benzene structure has a maximum of six nodes identified by letters and numbers; for instance, in this configuration, as '*a*' and '*b*' sub-networks, with point X_i indicating the coupling point of the two, where *i* is the number of coupling points in each.

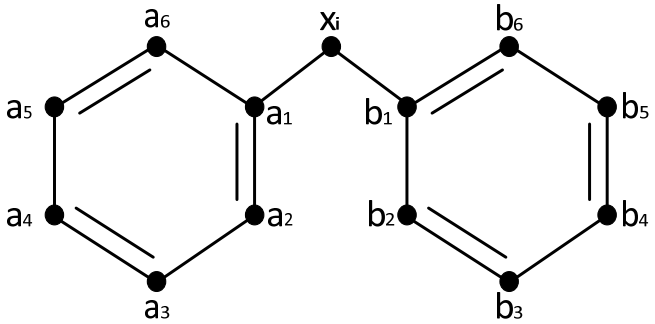

Figure 2. Aromatic network—Configuration 1 (DDT).

Spanning Tree for DDT Structure

For the configuration of the aromatic network with a DDT structure, it is essential to first configure its benzene structure considering that α_l is a variable for the overall connection status of each benzene structure and a binary variable representing the connection between two adjacent nodes. The conditions for network radiality are based on the concept that every node, except the root (sub-station node), has exactly one parent node but, in ring, mesh and aromatic networks, there is more than one parent node. It is considered that, in the case of a fault, an aromatic network will work like a radial one which is expressed by the following constraints:

$$\alpha_l = (a_n a_m + a_m a_n), \quad l = 1, 2. \tag{1}$$

Equation (1) shows the generic configuration for a network where:

$$\sum_{m \in N(n)} a_{nm} = \sum_{m \in N(n)} a_{mn} = k \tag{2}$$

Equation (2) indicates a network structure with a value of k. If this value is equal to 1, each node except the root one has exactly one parent which indicates a radial network and, if it is more than 1, the network is not a radial one. Therefore, when a benzene structure "*a*" is connected to a slack bus (CCP), Equation (1) will be:

$$\alpha_1 = (a_{nm} + a_{mn}) + (a_n x_i + x_i a_n) \tag{3}$$

where, the value of k is more than 1 and X_i represents the node of the slack bus. Figure 2 shows the structure of an Aromatic DDT network, the configuration of which is presented in Equations (4) and (5) based on Equation (1).

$$\begin{aligned}\alpha_1 = {} & (a_1a_2 + a_2a_1) + (a_2a_3 + a_3a_2) + (a_3a_4 + a_4a_3) + (a_4a_5 + a_5a_4) + (a_5a_6 + a_6a_5) + \\ & (a_6a_1 + a_1a_6) + (a_1x_i + x_ia_1)\end{aligned} \tag{4}$$

$$\begin{aligned}\alpha_2 = {} & (b_1b_2 + b_2b_1) + (b_2b_3 + b_3b_2) + (b_3b_4 + b_4b_3) + (b_4b_5 + b_5b_4) + \\ & (b_5b_6 + b_6b_5) + (b_6b_1 + b_1b_6) + (b_1x_i + x_ib_1)\end{aligned} \tag{5}$$

where 'a' and 'b' are the specific (sub-network) benzene structures and the suffixes their nodes, a_1a_2 is a binary variable that equals one if bus a_2 is the parent of bus a_1 and zero otherwise. Similarly, a_2a_3 is a binary variable equal to 1 if bus a_3 is the parent of bus a_2 and 0 otherwise, and so on, and Equation (6) is the overall configuration of an aromatic network (DDT) which connects two benzene structures through the coupling point (x_i).

The overall connection status of the DDT configuration is then:

$$\alpha_{Fcon1} = \alpha_1 + \alpha_2 \tag{6}$$

where α_1 and α_2 are the configurations of benzene structures 'a' and 'b' which are connected to the coupling point x_i. The real and reactive power balance of each bus is represented by:

$$p_n - \sum_{m \in N(n)} p_n p_m = P_n^D \quad \forall n \in N \tag{7}$$

$$q_n - \sum_{m \in N(n)} q_n q_m = Q_n^D \quad \forall n \in N \tag{8}$$

where p_n is the real power injected at bus n (n = 1,2, . . . , 6), ${P_n}^D$ the forecast real power demand at bus n, q_n the reactive power injected at bus n (n = 1,2, . . . , 6), ${Q_n}^D$ the forecast reactive power demand at bus n, N the set of buses and N(n) the set of buses connected to bus n.

$$p_n \le P_{max_n} \quad \forall n \in N_s \tag{9}$$

$$q_n \le Q_{max_n} \quad \forall n \in N_s \tag{10}$$

Equations (9) and (10) determine the capacity of the PCC (X_i), where P_{max_n} is the maximum real power allowed at the PCC, Q_{max_n} is the maximum reactive power allowed at the PCC and N_s is the set of sub-stations which is a subset of N.

The power flow equations and their convex relaxations are expressed as:

$$p_n p_m = \sqrt{2} G_L u_n^L - G_L r_L - B_L t_L \tag{11}$$

$$p_m p_n = \sqrt{2} G_L u_m^L - G_L r_L - B_L t_L \tag{12}$$

$$q_n q_m = -\sqrt{2} B_L u_n^L + B_L r_L + G_L t_L \tag{13}$$

$$q_m q_n = -\sqrt{2} B_L u_m^L + B_L r_L + G_L t_L \tag{14}$$

$$r_L^2 + t_L^2 \leq 2 u_n^L u_m^L \tag{15}$$

where $p_n p_m$ and $q_n q_m$ are the real and reactive power flows from bus n to bus m respectively, G_L is the conductance of line L, u_n^L and u_m^L are the auxiliary variables introduced in the convex relaxations of the equations for the ac power flow, r_L is a variable introduced in the convex relaxations of the ac power flow equations which corresponds to $v_n v_m \cos(\theta_n - \theta_m)$, where $v_n v_m$ are voltages and θ_n, θ_m the voltage angles of the two terminal buses (n and $n+1$) of line L and t_L a variable introduced in the convex relaxations of the ac power flow equations which corresponds to $v_n v_m \sin(\theta_n - \theta_m)$.

$$0 \leq u_n^L \leq \frac{V_{max_n}^2}{\sqrt{2}} \alpha_{Fconi} \tag{16}$$

$$0 \leq u_m^L \leq \frac{V_{max_m}^2}{\sqrt{2}} \alpha_{Fconi} \tag{17}$$

$$0 \leq u_n - u_n^L \leq \frac{V_{max_n}^2}{\sqrt{2}} (1 - \alpha_{Fconi}) \tag{18}$$

$$0 \leq u_m - u_m^L \leq \frac{V_{max_m}^2}{\sqrt{2}} (1 - \alpha_{Fconi}) \tag{19}$$

Equations (16)–(19) link the network configuration variable (α_{Fconi}) to the auxiliary variables (u_n^L, u_m^L) while Equations (20)–(25) determine the limits of the current and voltage flows.

$$u_n^L + u_m^L - \sqrt{2} r_1 \leq \frac{I_{max,L}^2}{\sqrt{2}(G_1^2 + B_1^2)} \tag{20}$$

$$P_n \geq 0; \quad \forall n \in N \tag{21}$$

$$O \leq r_1 \leq V_{max_n} V_{max_m} \tag{22}$$

$$-V_{max_n} V_{max_m} \leq t_1 \leq V_{max_n} V_{max_m} \tag{23}$$

$$\frac{V_{min_n}^2}{\sqrt{2}} \leq u_n \leq \frac{V_{max_n}^2}{\sqrt{2}}; \quad \forall n \in N \tag{24}$$

$$u_n^L, u_m^L \geq 0 \tag{25}$$

where V_{max_n} is the maximum voltage allowed at bus n, V_{min_n} is the minimum voltage allowed at bus n and $I_{max,L}^2$ is the maximum current flow allowed on line L.

The aforementioned equations provide the load flow of an aromatic network which, in the case of a fault, needs to be reconfigured. In this paper, a case scenario has been considered that the network will work like a radial network with multiple faults in the structure when the faults occur in single-bond overhead lines and the respective lines will be disconnected. Open circuit faults considering broken conductors are applied to lines connecting nodes a_1 and a_6 for benzene "a" and line connecting nodes b_1 and b_2 for benzene "b" as shown in Figure 3.

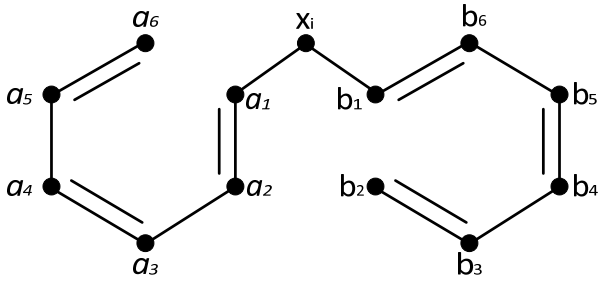

Figure 3. Aromatic network as radial network—Configuration 1.

Therefore, this DDT network's reconfiguration can be expressed by modifying Equations (4)–(6) as (26).

$$\begin{aligned}\alpha_{\text{Fco1}} = {} & (a_1a_2 + a_2a_1) + (a_2a_3 + a_3a_2) + (a_3a_4 + a_4a_3) + (a_4a_5 + a_5a_4) + \\ & (a_5a_6 + a_6a_5) + (a_1x_i + x_ia_1) + (b_2b_3 + b_3b_2) + (b_3b_4 + b_4b_3) + (b_4b_5 + b_5b_4) + \\ & (b_5b_6 + b_6b_5) + (b_6b_1 + b_1b_6) + (b_1x_i + x_ib_1)\end{aligned} \tag{26}$$

However, if a fault occurs in double-bond lines, these overhead lines will be replaced by underground cables with the modified Aromatic configuration shown in Figure 3 (self-healed network) represented by Equations (27)–(29).

$$\begin{aligned}\alpha'_1 = {} & (a'_1a'_2 + a'_2a'_1) + (a_2a_3 + a_3a_2) + (a'_3a'_4 + a'_4a'_3) + (a_4a_5 + a_5a_4) + \\ & (a'_5a'_6 + a'_6a'_5) + (a_6a_1 + a_1a_6) + (a_1x_i + x_ia_1)\end{aligned} \tag{27}$$

$$\begin{aligned}\alpha'_2 = {} & (b_1b_2 + b_2b_1) + (b'_2b'_3 + b'_3b'_2) + (b_3b_4 + b_4b_3) + (b'_4b'_5 + b'_5b'_4) + \\ & (b_5b_6 + b_6b_5) + (b'_6b'_1 + b'_1b'_6) + (b_1x_i + x_ib_1)\end{aligned} \tag{28}$$

$$\alpha'_{\text{Fcon1}} = \alpha'_1 + \alpha'_2 \tag{29}$$

where $a'_1a'_2$, $a'_3a'_4$ and $a'_5a'_6$, and $b'_2b'_3$, $b'_4b'_5$ and $b'_6b'_1$ represent the underground cables in benzene structures 'a' and 'b' respectively.

The original DDT based aromatic network has been designed considering the Institute of Electrical and Electronics Engineers (IEEE) 13 bus test system. However, it has not been justified if the original aromatic network could be scaled to a larger network to be implemented in a real environment. To justify this, another level of benzene network has been added to the DDT network forming a triphenylmethanol structure as shown in the following section.

3.2. Aromatic Network—Configuration 2 (Triphenylmethanol)

Triphenylmethanol contains three benzene structures and an alcohol group bound to a central tetrahedral carbon atom. Therefore, to connect an additional benzene structure to configuration 1 (DDT), a triphenylmethanol structure is used. The schematic of this configuration as shown in Figure 4, which has another set of benzene structures (c) added to the network as expressed in (30) and (31):

$$\begin{aligned}\alpha_3 = {} & (c_1c_2 + c_2c_1) + (c_2c_3 + c_3c_2) + (c_3c_4 + c_4c_3) + (c_4c_5 + c_5c_4) + (c_5c_6 + c_6c_5) \\ & + (c_6c_1 + c_1c_6) + (c_1x_i + x_ic_1)\end{aligned} \tag{30}$$

$$\alpha_{\text{Fcon2}} = \alpha_1 + \alpha_2 + \alpha_3 \tag{31}$$

where c_1c_2, c_2c_3, c_3c_4, c_4c_5 and c_5c_6 represents overhead connections of benzene structure 'c'.

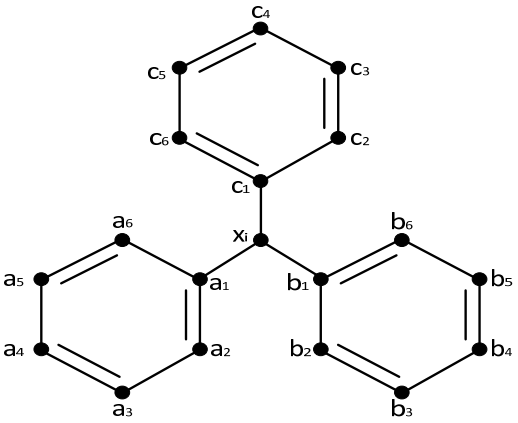

Figure 4. Aromatic network—Configuration 2.

As this research is conducted based on considering that faults will occur and the configuration of the aromatic network will be like that of a radial one, three different faults are applied in this triphenylmethanol structure (configuration 2) to make it radial (considering that these damages have been done due to the natural disaster), as shown in Figure 5. A fault at each benzene structure has been introduced by disconnecting the lines between nodes a_1 and a_6 for benzene "a" b_1 and b_2 for benzene "b" and c_1 and c_2 for benzene "c"

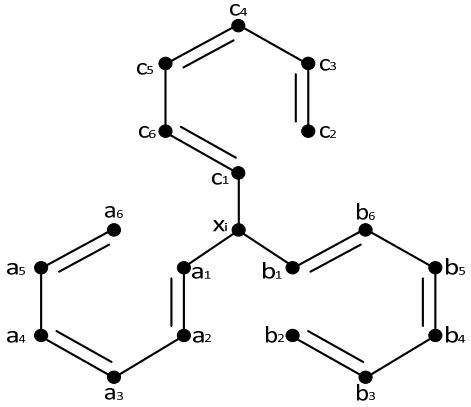

Figure 5. Aromatic network as radial network—Configuration 2.

The overall configuration of this triphenylmethanol network during a fault is expressed as (32).

$$\begin{aligned}\alpha'_{Fco2} = {} & (a_1a_2 + a_2a_1) + (a_2a_3 + a_3a_2) + (a_3a_4 + a_4a_3) + (a_4a_5 + a_5a_4) + (a_5a_6 + a_6a_5) \\ & + (a_1x_i + x_ia_1) + (b_2b_3 + b_3b_2) + (b_3b_4 + b_4b_3) + (b_4b_5 + b_5b_4) + (b_5b_6 + b_6b_5) + \\ & (b_6b_1 + b_1b_6) + (b_1x_i + x_ib_1) + (c_2c_3 + c_3c_2) + (c_3c_4 + c_4c_3) + (c_4c_5 + c_5c_4) + \\ & (c_5c_6 + c_6c_5) + (c_6c_1 + c_1c_6) + (c_1x_i + x_ic_1)\end{aligned} \quad (32)$$

3.3. Aromatic Network–Configuration 3 (Acenaphthylene)

Acenaphthylene is a polycyclic aromatic hydrocarbon in which every atom in the ring is conjugated and in a form of a flat planner molecule. An additional overhead line and an underground cable are added to the Aromatic DDT network to obtain this acenaphthylene structure for a power distribution network. This structure is suitable for small islands with high load demands where the utility grid is not available, the slack bus will be supported by the DGs. The acenaphthylene structure can effectively handle high load demands with minimum or no voltage profile issues with the help of an extra

overhead and transmission line connecting a_3 and b_3 of the original DDT structure. Figure 6 shows that a_3 and b_3 are connected to achieve this structure which is represented as:

$$\alpha_{Fcon3} = \alpha_1 + \alpha_2 + \alpha_4 \tag{33}$$

where $\alpha_4 = (a_3b_3 + b_3a_3)$

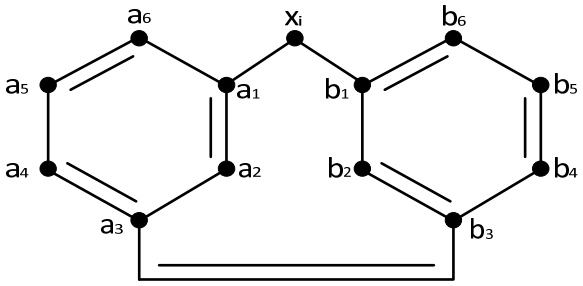

Figure 6. Aromatic network—Configuration 3.

This network is capable of handling more than one fault until it achieves a minimum radial structure. In this case, the worst-case scenario is considered by applying three broken conductors (between nodes a_1 and a_3 for benzene "a", b_1 and b_2, b_3 and b_4 for benzene "b") on the acenaphthylene structure, as shown in Figure 7, to obtain a so-called radial system.

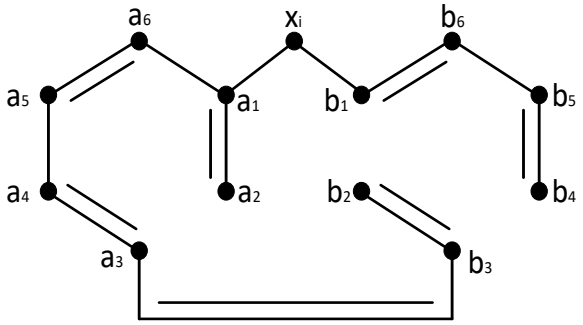

Figure 7. Aromatic network as radial network—Configuration 3.

The expression for the final configuration of the acenaphthylene network with faults is represented using (34).

$$\begin{aligned}\alpha'_{Fco3} = {} & (a_3a_4 + a_4a_3) + (a_4a_5 + a_5a_4) + (a_5a_6 + a_6a_5) + (a_6a_1 + a_1a_6) + (a_1a_2 + a_2a_1) \\ & + (a_1x_i + x_ia_1) + (b_2b_3 + b_3b_2) + (a_3b_3 + b_3a_3) + (b_4b_5 + b_5b_4) + (b_5b_6 + b_6b_5) + \\ & (b_6b_1 + b_1b_6) + (b_1x_i + x_ib_1)\end{aligned} \tag{34}$$

A summary based on the above equations of all aromatic network configurations and reconfigurations have been shown in Table 1. The decision parameters "1" and "0" represent the connection status to determine how the network is configured ("1" signifies connect while "0" disconnect).

Table 1. Connection status of aromatic network configurations and reconfigurations.

Decision Variable	DDT Structure	Reconfigured DDT Structure	Triphenylmethanol Structure	Reconfigured Triphenylmethanol	Acenaphthylene Structure	Reconfigured Acenaphthylene Structure
a1a2	1	1	1	1	1	1
a2a1	1	1	1	1	1	1
a2a3	1	1	1	1	1	0
a3a2	1	1	1	1	1	0
a3a4	1	1	1	1	1	1
a4a3	1	1	1	1	1	1
a4a5	1	1	1	1	1	1
a5a4	1	1	1	1	1	1
a5a6	1	1	1	1	1	1
a6a5	1	1	1	1	1	1
a6a1	1	0	1	0	1	1
a1a6	1	0	1	0	1	1
a1xi	1	1	1	1	1	1
xia1	1	1	1	1	1	1
b1xi	1	1	1	1	1	1
xib1	1	1	1	1	1	1
b1b2	1	0	1	0	1	0
b2b1	1	0	1	0	1	0
b2b3	1	1	1	1	1	1
b3b2	1	1	1	1	1	1
b3b4	1	1	1	1	1	0
b4b3	1	1	1	1	1	0
b4b5	1	1	1	1	1	1
b5b4	1	1	1	1	1	1
b5b6	1	1	1	1	1	1
b6b5	1	1	1	1	1	1
b6b1	1	1	1	1	1	1
b1b6	1	1	1	1	1	1
xic1	0	0	1	1	0	0
c1xi	0	0	1	1	0	0
c1c2	0	0	1	0	0	0
c2c1	0	0	1	0	0	0
c2c3	0	0	1	1	0	0
c3c2	0	0	1	1	0	0
c3c4	0	0	1	1	0	0
c4c3	0	0	1	1	0	0
c4c5	0	0	1	1	0	0
c5c4	0	0	1	1	0	0
c5c6	0	0	1	1	0	0
c6c5	0	0	1	1	0	0
c6c1	0	0	1	1	0	0
c1c6	0	0	1	1	0	0
a3b3	0	0	0	0	1	1
b3a3	0	0	0	0	1	1

4. Analysis and Discussion

The three configurations were set up in a simulation environment using the Electrical Transient and Analysis Program (ETAP) software, load flow and harmonics analyses were conducted, and the results presented in this section. The reconfigured networks (faulted networks) were also simulated at various fault scenarios as described in Section 3. The load flow of the original and the faulted structures were done to determine the impact of faults on each network, whereas harmonics analysis was done to determine the quality of each structure. The results of the aromatic network configurations are then compared with the existing radial, ring and mesh networks in this section to justify the performance of each aromatic network configuration.

4.1. Load Flow Analysis

To evaluate the load flows of different configurations for the aromatic distribution networks, the aforementioned equations for load flow were used. Both a configuration's normal operating and faulty conditions (radial structure) were used to determine its load flow in order to understand the network's performances in these situations.

4.1.1. Load Flow of Configuration 1 (DDT)

The basic configuration of aromatic network (DDT structure) was set up in an ETAP software environment as configuration 1, as shown in Figure 8. Its design is a modified version of an IEEE 13-bus radial distribution network [37,38,40]. Although the buses were renumbered from 100 to 112 and follow a unique numbering pattern, their ratings are similar to those of the IEEE 13-bus radial network. The basic aromatic network was implemented to compare its performance with the traditional networks (radial, ring and mesh from the previous research in [38]) and other aromatic configurations (based on triphenylmethanol and acenaphthylene structures).

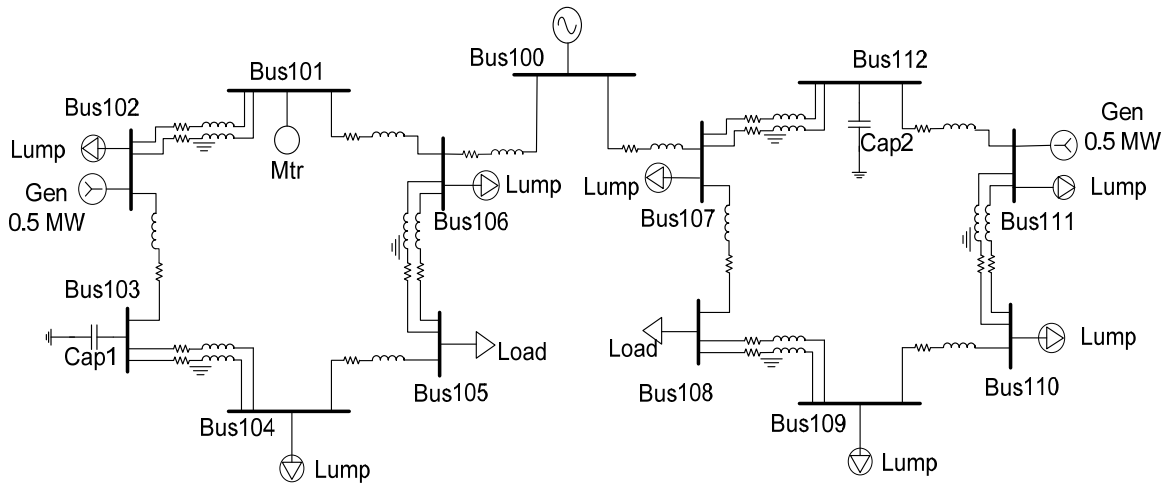

Figure 8. Aromatic network—Configuration 1 (DDT) in ETAP.

It can be seen from Table 2, that only one marginal voltage bus (under the normal operation of the DDT structure) had an operating voltage of 102.67% indicating that Bus 100 (the slack bus) had an over-voltage. The marginal and critical voltage limits used in this section are those considered in [38] and all the buses are rated as 4.16 kV. Table 2 shows the real and reactive power loadings of each bus, with the maximum ones of the slack bus 3.031 MW and 1.455 MVar respectively. It was observed that the network performed well in both the DDT and radial structures (reconfigured network). However, the voltage profile in the reconfigured one was slightly poor considering variations in its voltage level and lower-end voltages, with Buses 109, 110 and 111 having slightly lower voltages.

Table 2. Load flow of aromatic networks.

Bus ID	MW Loading			MVar Loading			Voltage at Aromatic Configuration			Voltage of Reconfigured Networks		
	Con. 1	Con. 2	Con. 3	Con. 1	Con. 2	Con. 3	Con. 1	Con. 2	Con. 3	Con. 1	Con. 2	Con. 3
Bus 100	3.031	3.776	3.031	1.455	2.261	1.455	102.67	102.67	102.67	102.67	102.67	102.67
Bus 101	1.218	0.201	1.218	0.88	0.094	0.88	101.93	101.89	101.93	101.78	101.78	100.7
Bus 102	1.033	0.5	1.033	0.797	0.082	0.797	101.6	101.92	101.6	101.83	101.83	100.43
Bus 103	0.792	0.126	0.792	0.759	0.104	0.759	101.08	101.91	101.08	101.85	101.85	99.82
Bus 104	1.29	0.126	1.29	0.757	0.058	0.757	100.8	101.88	100.8	101.84	101.84	99.5
Bus 105	1.284	0.133	1.284	0.752	0.11	0.752	100.28	101.88	100.28	101.85	101.85	101.29
Bus 106	1.154	1.261	1.154	0.659	0.864	0.659	99.95	101.93	99.95	101.93	101.93	101.33
Bus 107	1.696	0.27	1.696	0.551	0.468	0.551	101.93	101.94	101.93	101.7	101.7	102.6
Bus 108	0.392	1.258	0.392	0.209	0.689	0.209	101.88	101.99	101.88	101.99	101.99	102.58
Bus 109	0.219	0.812	0.219	0.291	0.481	0.291	101.9	101.54	101.9	99.81	99.81	99.14
Bus 110	0.045	0.843	0.045	0.561	0.462	0.561	101.95	101.38	101.95	99.87	99.87	99.2
Bus 111	0.1	0.369	0.1	0.27	0.176	0.27	101.88	101.48	101.88	100.3	100.3	102.4
Bus 112	0.46	0.769	0.46	0.3	0.467	0.3	101.75	101.67	101.75	100.97	100.97	102.46
Bus 113	-	0.312	-	-	0.137	-	-	101.93	-	-	101.89	-
Bus 114	-	0.173	-	-	0.185	-	-	101.92	-	-	101.8	-
Bus 115	-	0.1	-	-	0.418	-	-	101.97	-	-	101.81	-
Bus 116	-	0.5	-	-	0.29	-	-	101.91	-	-	101.67	-
Bus 117	-	0.1	-	-	0.115	-	-	101.94	-	-	101.61	-
Bus 118	-	1.255	-	-	0.683	-	-	101.99	-	-	102	-

4.1.2. Load Flow of Configuration 2 (Triphenylmethanol)

The software setup for configuration 2 is shown in Figure 9, in which another set of benzene structure was connected to the aromatic DDT network at the PCC (Bus 100) to obtain a triphenylmethanol structure, the performance of which was evaluated. Since the buses in this structure follow the same pattern as in the DDT one, they were numbered from 100 to 118.

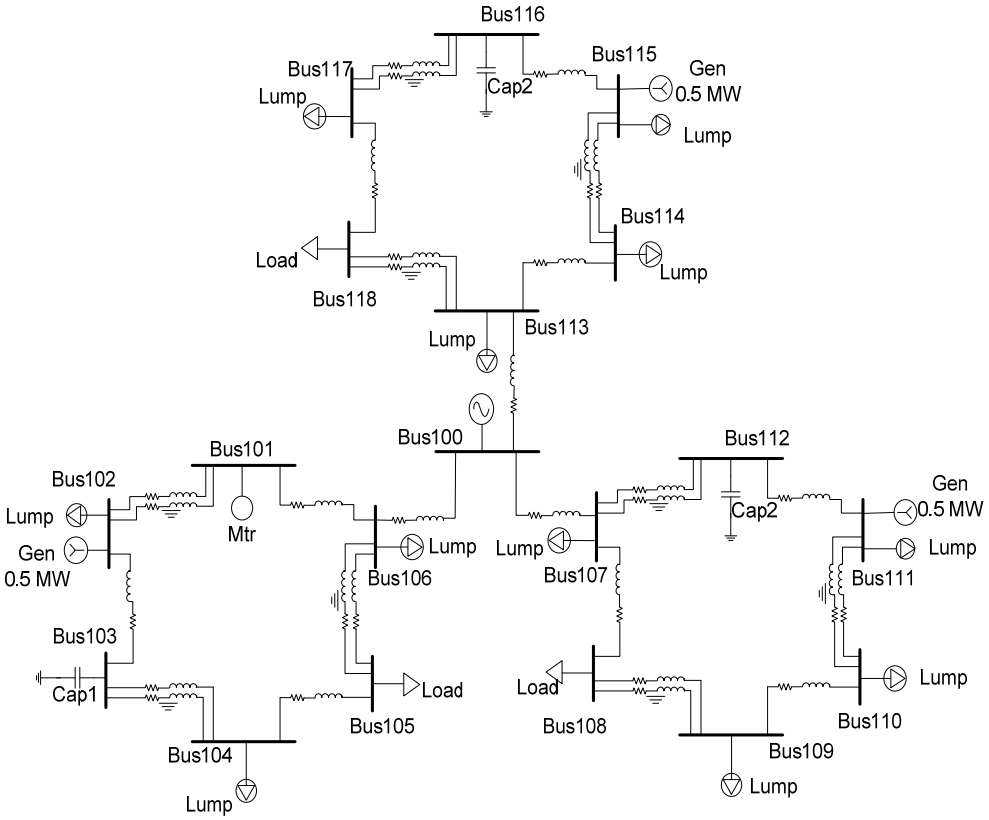

Figure 9. Aromatic network—Configuration 2 (triphenylmethanol) in ETAP.

A load flow analysis of the normal and reconfigured Triphenylmethanol structures was conducted and the results presented in Table 2.

These results show that the number of marginal buses remained the same as in the DDT network under normal operation. This indicates that adding another level of benzene structure does not significantly affect the voltage profile of the aromatic network operating normally as a triphenylmethanol structure. However, the number of marginal buses increased for the faulty triphenylmethanol structure operating as a radial network.

4.1.3. Load Flow of Configuration 3 (Acenaphthylene)

The acenaphthylene-based structure of an aromatic network in the simulation environment is shown in Figure 10 in which the DDT one had additional transmission lines (both underground and overhead) to connect Buses 104 and 109.

A load flow analysis of the acenaphthylene configuration shows that the only marginal bus for the acenaphthylene structure is the slack one under normal operating conditions. The acenaphthylene structure was much better under normal than reconfigured conditions (radial structure made from acenaphthylene) when the number of marginal buses increased to 5. Buses 100, 107, 108, 111 and 112 suffered from over-voltage issues with operating voltages of 102.67%, 102.6%, 102.58%, 102.4% and 102.46%, respectively. Voltage drops were observed at the lower-end buses of the radial configuration (Buses 103, 104, 109 and 110), as shown in Table 2.

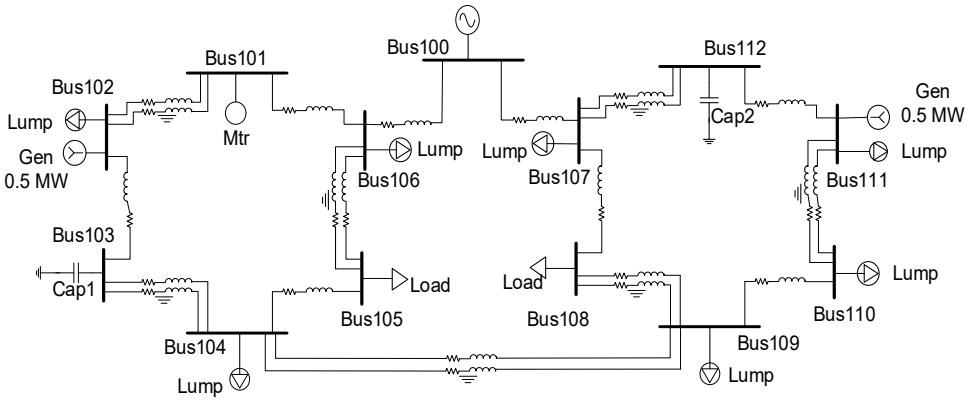

Figure 10. Aromatic network—Configuration 3 (acenaphthylene) in ETAP.

Table 3 presents load flow results of the existing distribution networks [38]. The results from classical networks (radial, ring and mesh) have then been compared to the aromatic network configurations (Table 2) and it have been found that the voltage profile of each aromatic network configuration is more stable in terms of critical bus number and voltage level in the network.

Table 3. Load flow of existing networks.

Bus ID	MW Loading			MVar Loading			Voltage at Classic Networks		
	Radial	Ring	Mesh	Radial	Ring	Mesh	Radial	Ring	Mesh
Bus 632	3.528	2.547	2.520	1.467	1.472	1.378	102.56	102.67	102.67
Bus 633	0.405	0.585	1.222	0.300	0.424	0.668	102.31	102.31	102.01
Bus 634	0.400	0.574	0.592	0.290	0.404	0.344	100.28	99.41	101.69
Bus 645	0.424	1.846	1.187	0.217	0.970	0.637	102.34	101.69	102.04
Bus 646	0.240	1.652	0.339	0.138	0.876	0.202	102.21	100.80	101.85
Bus 652	0.128	0.126	0.132	0.086	0.085	0.089	100.26	99.29	101.72
Bus 671	2.569	0.598	1.584	0.796	0.717	0.719	100.44	98.55	101.69
Bus 675	0.843	0.843	0.843	0.603	0.683	0.662	100.24	98.41	101.56
Bus 680	0.000	0.000	0.000	0.000	0.000	0.000	100.44	98.55	101.69
Bus 684	0.299	1.734	0.500	0.086	0.743	0.089	100.32	99.34	101.78
Bus 685	0.170	1.415	0.173	0.101	0.832	0.169	100.27	100.05	101.79
Bus 692	1.015	0.844	0.830	0.151	0.220	0.199	100.44	98.55	101.69

A distribution network operates directly with its load and suffers from power quality issues [41]. Configuration of the network has an impact on power quality. One indicator of power quality is the presence of harmonics in the network. The next section discusses the harmonics analyses conducted to understand the power quality in the aromatic networks with the various configurations previously designed.

4.2. Harmonic Analyses of Aromatic Configurations

Two major indicators of harmonic distortions used in this research are the total harmonic distortion (THD) and the individual harmonic distortion (IHD).

The THD is the ratio of the rms of all the harmonics to the fundamental component and IHD the ratio of the given harmonics to the fundamental one, as defined in Equations (35) and (36), respectively.

$$\mathrm{THD} = \frac{\sqrt{\sum_{2}^{\infty} \mathrm{F^2}_i}}{\mathrm{F}_i} \tag{35}$$

$$\mathrm{IHD} = \frac{\mathrm{F}_i}{\mathrm{F}_1} \tag{36}$$

Harmonics analyses of the DDT configurations and radial conditions are performed with the results presented in Tables 4 and 5 for Voltage IHDs (VIHDs) and Voltage THDs (VTHDs), respectively.

Table 4. VIHDs of aromatic networks.

Bus ID	VIHD at Aromatic Configuration (%)			VIHD at Reconfigured Configuration (%)			Order
	Con1	Con2	Con3	Con1	Con2	Con3	
Bus100	2.92	4.75	2.93	2.91	4.78	2.92	5
Bus101	3.58	5.38	3.61	4.42	6.22	3.72	5
Bus102	3.71	5.51	3.75	-	6.23	3.94	5
Bus103	3.44	5.41	3.64	4.06	5.89	3.97	5
Bus104	3.53	5.33	3.57	3.86	5.69	3.97	5
Bus105	3.44	5.24	3.47	3.61	5.45	3.32	5
Bus106	3.32	5.13	3.35	3.30	5.16	3.32	5
Bus107	3.63	5.52	3.61	3.66	5.60	3.69	5
Bus108	3.43	5.30	3.42	3.41	5.32	3.43	5
Bus109	3.55	5.42	3.52	4.04	5.94	3.97	5
Bus110	3.62	5.48	3.58	4.04	5.94	3.97	5
Bus111	3.69	5.56	3.66	4.04	5.94	4.07	5
Bus112	3.89	5.75	3.86	4.04	5.95	4.07	5
Bus113	-	5.45	-	-	5.66	-	5
Bus114	-	5.74	-	-	6.25	-	5
Bus115	-	5.88	-	-	6.55	-	5
Bus116	-	5.94	-	-	6.91	-	5
Bus117	-	5.49	-	-	6.91	-	5
Bus118	-	5.31	-	-	5.36	-	5
Bus100	-	2.79	1.65	-	2.81	1.65	7
Bus101	-	3.04	1.99	-	3.36	2.03	7
Bus102	-	3.09	2.06	-	3.37	2.13	7
Bus103	-	3.07	2.03	-	3.26	2.17	7
Bus104	-	3.04	1.99	-	3.18	2.17	7
Bus105	-	3.00	1.93	-	3.08	1.84	7
Bus106	-	2.94	1.86	-	2.96	1.84	7
Bus107	-	3.28	2.06	-	3.32	2.13	7
Bus108	-	3.13	1.94	-	3.15	1.97	7
Bus109	-	3.19	1.98	-	3.41	2.17	7
Bus110	-	3.22	2.00	-	3.41	2.17	7
Bus111	-	3.25	2.05	-	3.41	2.29	7
Bus112	-	3.34	2.15	-	3.42	2.29	7
Bus113	-	3.26	-	-	3.40	-	7
Bus114	-	3.47	-	-	3.80	-	7
Bus115	-	3.57	-	-	4.00	-	7
Bus116	-	3.51	-	-	4.10	-	7
Bus117	-	3.26	-	-	4.10	-	7
Bus118	-	3.16	-	-	3.20	-	7
Bus100	-	-	1.88	-	-	1.97	11
Bus101	-	-	2.13	-	-	2.16	11
Bus102	-	-	2.17	-	-	2.21	11
Bus103	-	-	2.23	-	-	2.30	11
Bus104	-	-	2.21	-	-	2.30	11
Bus105	-	-	2.14	-	-	2.06	11
Bus106	-	-	2.06	-	-	2.06	11
Bus107	-	1.72	2.45	-	1.61	2.72	11
Bus108	-	1.61	2.26	-	1.52	2.47	11
Bus109	-	-	2.25	-	-	2.30	11
Bus110	-	-	2.25	-	-	2.30	11
Bus111	-	-	2.29	-	-	2.73	11
Bus112	-	-	2.40	-	-	2.73	11

The VIHDs of the aromatic DDT structures (configuration 1 to 3) are presented in Table 4 in which the voltage distortions and their corresponding harmonic orders are given for both the normal DDT structure and the reconfigured one operating as a radial network. These networks have an impact on the 5th, 7th and 11th order harmonics.

The VTHD results for the voltage distortion fundamentals and VTHD percentages of the aromatic and reconfigured structures are presented in Table 5. In most of the cases, the aromatic structures are better than the reconfigured (radial) network in terms of VIHDs and VTHD. The voltage distortion

fundamental is within the limits for aromatic and for reconfigured configurations, however, a slight voltage drop has been observed for the reconfigured configurations.

Table 5. VTHDs of aromatic networks.

Bus ID	Voltage Distortion Fundamental at Original Config.			VTHD (%) at Original Configuration			Voltage Distortion Fundamental at Reconfigured Config.			VTHD (%) at Reconfigured Configuration		
	Con1	Con2	Con3	Con1	Con2	Con3	Con1	Con2	Con3	Con1	Con2	Con3
Bus100	-	102.67	102.67	-	5.70	3.94	-	102.67	102.67	-	5.72	3.98
Bus101	-	101.89	101.75	-	6.33	4.72	-	101.78	100.70	-	7.20	4.82
Bus102	-	101.92	101.76	-	6.46	4.87	-	101.83	100.43	-	7.21	5.05
Bus103	101.79	101.91	101.71	4.64	6.38	4.82	101.85	101.85	99.82	5.15	6.87	5.14
Bus104	101.75	101.88	101.67	4.55	6.30	4.74	101.84	101.84	99.50	4.92	6.66	5.14
Bus105	101.56	101.88	101.73	4.44	6.21	4.61	101.85	101.85	101.29	4.63	6.40	4.39
Bus106	101.48	101.93	101.81	4.31	6.09	4.43	101.93	101.93	101.33	4.29	6.10	4.39
Bus107	-	101.94	102.07	-	6.68	4.97	-	101.70	102.60	-	6.75	5.22
Bus108	-	101.99	102.11	-	6.39	4.65	-	101.99	102.58	-	6.41	4.80
Bus109	-	101.54	101.74	-	6.52	4.74	-	99.81	99.14	-	7.04	5.14
Bus110	-	101.38	101.61	-	6.58	4.78	-	99.87	99.20	-	7.04	5.14
Bus111	-	101.48	101.69	-	6.66	4.88	-	100.30	102.40	-	7.04	5.53
Bus112	-	101.67	101.84	-	6.87	5.14	-	100.97	102.46	-	7.05	5.53
Bus113	-	101.93	-	-	6.63	-	-	101.89	-	-	6.87	-
Bus114	-	101.92	-	-	7.03	-	-	101.80	-	-	7.65	-
Bus115	-	101.97	-	-	7.23	-	-	101.81	-	-	8.05	-
Bus116	-	101.91	-	-	7.19	-	-	101.67	-	-	8.35	-
Bus117	-	101.94	-	-	6.65	-	-	101.61	-	-	8.35	-
Bus118	-	102.00	-	-	6.44	-	-	102.00	-	-	6.49	-

In this work, various aromatic distribution networks were analyzed. Firstly, one based on the concept of DDT was configured and a load flow analysis conducted. It was determined that, using the configuration method defined in Equations (1)–(38), its load flow could find acceptable levels of the operating voltage and power while a harmonics analysis found that it has marginal 5th order harmonics.

Configuration 2 is similar to configuration 1 but with an additional benzene structure at the slack bus. The load flow results were within the limits which indicate that the DDT based aromatic network could be scaled and implemented in larger suburbs/communities without having any voltage issues.

Similarly, for configuration 3 (acenaphthylene), the load flow shows that the system operated with an over-voltage at the slack bus (Bus100) while the harmonics levels of all the buses were within acceptable limits.

5. Conclusions

In this paper, constructing aromatic distribution networks using a configuration technique is explained. As in previous work, it is observed that an aromatic network with a DDT structure is more efficient and attractive than other existing ones, with reconfigured aromatic networks and analyses of their load flows and harmonics analysis included in this work. The simulation results are promising and prove that structures based on an aromatic network are flexible and provide the freedom for utility companies to reconfigure from one aromatic structure to another without reducing a system's performance. The computational results demonstrate that an aromatic network could be the best option for future designs of smart grids in proving sustainable energy. The aromatic network designs have been presented to few companies who have shown interest; however, it will take few years to implement a new aromatic network in real time as more validation apart from voltage stability and power quality is required. Hence, a great deal of research for the implementation of aromatic networks is essential. Several issues, including economic viability, optimization of generation, energy storage and control technique, could be interesting topics for future work.

Author Contributions: K.P.—software, formal analysis, visualization, original draft preparation; K.A.M.—review and editing, project administration; H.R.P.—supervision, review and editing; F.R.I.—conceptualization, methodology, project administration and supervision. All authors have read and agreed to the published version of the manuscript.

Funding: This research received no external funding.

Conflicts of Interest: The authors declare no conflict of interest.

References

1. Gasser, P.; Lustenberger, P.; Cinelli, M.; Kim, W.; Spada, M.; Burgherr, P.; Sun, T.Y. A review on resilience assessment of energy systems. *Sustain. Resilient Infrastruct.* **2019**. [CrossRef]
2. Lin, P.; Wang, N.; Ellingwood, B.R. A risk de-aggregation framework that relates community resilience goals to building performance objectives. *Sustain. Resilient Infrastruct.* **2016**, *1*, 1–13. [CrossRef]
3. Wang, Y.; Chen, C.; Wang, J.; Baldick, R. Research on resilience of power systems under natural disasters—A review. *IEEE Trans. Power Syst.* **2015**, *31*, 1604–1613. [CrossRef]
4. Frohlich, T.C. From Elena to Katrina: These Are the Costliest Hurricanes to Ever Hit the US. Available online: https://www.usatoday.com/story/money/2018/09/12/%20most-destructive-hurricanes-of-all-time/36697269/ (accessed on 24 December 2019).
5. Li, Z.; Shahidehpour, M.; Aminifar, F.; Alabdulwahab, A.; AlTurki, Y. Networked microgrids for enhancing the power system resilience. *Proc. IEEE* **2017**, *105*, 1289–1310. [CrossRef]
6. Che, L.; Khodayar, M.; Shahidehpour, M. Only connect: Microgrids for distribution system restoration. *IEEE Power Energy Mag.* **2014**, *12*, 70–81.
7. CBS. Hurricane Harvey: Texas Power Outages Affect More than Quarter-Million. Available online: https://www.cbsnews.com/news/hurricane-harvey-texas-power-outages-affect-more-than-255000/ (accessed on 20 December 2019).
8. President's Council of Economic Advisers and the U.S. Department of Energy's Office of Electricity and Energy Reliability. *Economic Benefits of Increasing Electric Grid Resilience to Weather Outages*; Executive Office of the President of the United States: Washington, DC, USA, 2013.
9. Kavousi-Fard, A.; Wang, M.; Su, W. Stochastic resilient post-hurricane power system recovery based on mobile emergency resources and reconfigurable networked microgrids. *IEEE Access* **2018**, *6*, 72311–72326. [CrossRef]
10. Prakash, K.; Lallu, A.; Islam, F.R.; Mamun, K.A. Review of Power System Distribution Network Architecture. In Proceedings of the 2016 3rd Asia-Pacific World Congress on Computer Science and Engineering (APWC on CSE), Nadi, Fiji, 5–6 December 2016; pp. 124–130.
11. Civanlar, S.; Grainger, J.J.; Yin, H.; Lee, S.S.H. Distribution feeder reconfiguration for loss reduction. *IEEE Trans. Power Deliv.* **1988**, *3*, 1217–1223. [CrossRef]
12. Freitas, K.B.; Arantes, M.S.; Toledo, C.F.; Delbem, A.C. MIQP model and improvement heuristic for power loss minimization in distribution system with network reconfiguration. *J. Heuristics* **2020**, *26*, 59–81. [CrossRef]
13. Gangwar, P.; Singh, S.N.; Chakrabarti, S. Network reconfiguration for the DG-integrated unbalanced distribution system. *IET Gener. Transm. Distrib.* **2019**, *13*, 3896–3909. [CrossRef]
14. Abubakar, A.S.; Ekundayo, K.R.; Olaniyan, A.A. Optimal reconfiguration of radial distribution networks using improved genetic algorithm. *Niger. J. Technol. Dev.* **2019**, *16*, 10–16. [CrossRef]
15. Lin, W.M.; Cheng, F.S.; Tsay, M.T. Distribution feeder reconfiguration with refined genetic algorithm. *IEEE Proc.-Gener. Transm. Distrib.* **2000**, *147*, 349–354. [CrossRef]
16. Goswami, S.; Basu, S. A new algorithm for the reconfiguration of distribution feeders for loss minimization. *IEEE Trans. Power Deliv.* **1992**, *7*, 1484–1491. [CrossRef]
17. Shirmohammadi, D.; Hong, H.W. Reconfiguration of electric distribution networks for resistive line loss reduction. *IEEE Trans. Power Deliv.* **1989**, *4*, 1492–1498. [CrossRef]
18. Wagner, T.P.; Chikhani, A.Y.; Hackam, R. Feeder reconfiguration for loss reduction: An application of distribution automation. *IEEE Trans. Power Deliv.* **1991**, *6*, 1922–1931. [CrossRef]
19. Gomes, F.V.; Carneiro, S.; Pereira, J.L.R.; Vinagre, M.P.; Garcia, P.A.N.; De Araujo, L.R. A new distribution system reconfiguration approach using optimum power flow and sensitivity analysis for loss reduction. *IEEE Trans. Power Syst.* **2006**, *21*, 1616–1623. [CrossRef]
20. Raju, G.; Bijwe, P.R. An efficient algorithm for minimum loss reconfiguration of distribution system based on sensitivity and heuristics. *IEEE Trans. Power Syst.* **2008**, *23*, 1280–1287. [CrossRef]

21. Koziel, S.; Rojas, A.L.; Moskwa, S. Power Loss Reduction through Distribution Network Reconfiguration Using Feasibility-Preserving Simulated Annealing. In Proceedings of the 2018 19th International Scientific Conference on Electric Power Engineering (EPE), Brno, Czech Republic, 16–18 May 2018; pp. 1–5.
22. Chiang, H.D.; Rene, J.J. Optimal network reconfiguration in distribution systems. Part 1. A new formulation and a solution methodology. *IEEE Trans. Power Deliv.* **1990**, *5*, 1902–1908. [CrossRef]
23. Chiang, H.D.; Rene, J.J. Optimal network reconfiguration in distribution systems. Part 2. Solution algorithms and numerical results. *IEEE Trans. Power Deliv.* **1992**, *5*, 1568–1574. [CrossRef]
24. Muthukumar, K.; Jayalalitha, S. Integrated approach of network reconfiguration with distributed generation and shunt capacitors placement for power loss minimization in radial distribution networks. *Appl. Soft Comput.* **2017**, *52*, 1262–1284.
25. Murty, V.; Kumar, A. Optimal DG integration and network reconfiguration in microgrid system with realistic time varying load model using hybrid optimization. *IET Smart Grid* **2019**, *2*, 192–202. [CrossRef]
26. Huang, Y.C. Enhanced genetic algorithm-based fuzzy multi-objective approach to distribution network reconfiguration. *IEEE Proc.-Gener. Transm. Distrib.* **2002**, *149*, 615–620. [CrossRef]
27. Miguel, A.A.; Hern'an, S.H. Distribution network configuration for minimum energy supply cost. *IEEE Trans. Power Syst.* **2004**, *19*, 538–542.
28. Taleski, R.; Rajicic, D. Distribution network reconfiguration for energy loss reduction. *IEEE Trans. Power Syst.* **1997**, *12*, 398–406. [CrossRef]
29. Schmidt, H.; Ida, N.; Kagan, N.; Guaraldo, J. Fast reconfiguration of distribution systems considering loss minimization. *IEEE Trans. Power Syst.* **2005**, *20*, 1311–1319. [CrossRef]
30. Koutsoukis, N.C.; Siagkas, D.O.; Georgilakis, P.S.; Hatziargyriou, N.D. Online reconfiguration of active distribution networks for maximum integration of distributed generation. *IEEE Trans. Autom. Sci. Eng.* **2017**, *14*, 437–448. [CrossRef]
31. Shu, D.; Huang, Z.; Li, J.; Zou, X. Application of multi-agent particle swarm algorithm in distribution network reconfiguration. *Chin. J. Electron.* **2016**, *25*, 1179–1185. [CrossRef]
32. Larimi, S.M.; Haghifam, M.R.; Moradkhani, A. Risk-based reconfiguration of active electric distribution networks. *IET Gener. Transm. Distrib.* **2016**, *10*, 1006–1015. [CrossRef]
33. Jazebi, S.; Hadji, M.M.; Naghizadeh, R.A. Distribution network reconfiguration in the presence of harmonic loads: Optimization techniques and analysis. *IEEE Trans. Smart Grid* **2014**, *5*, 1929–1937. [CrossRef]
34. Bernardon, D.P.; Garcia, V.J.; Ferreira, A.S.; Canha, L.N. Multicriteria distribution network reconfiguration considering sub-transmission analysis. *IEEE Trans. Power Deliv.* **2010**, *25*, 2684–2691. [CrossRef]
35. Lee, C.; Liu, C.; Mehrotra, S.; Bie, Z. Robust distribution network reconfiguration. *IEEE Trans. Smart Grid* **2015**, *6*, 836–842. [CrossRef]
36. Pham, T.H.; Besanger, Y.; Hadjsaid, N. New challenges in power system restoration with large scale of dispersed generation insertion. *IEEE Trans. Power Syst.* **2009**, *24*, 398–406. [CrossRef]
37. Islam, F.R.; Mamun, K.A.; Prakash, K.; Lallu, A. *Aromatic Network for Power Distribution System*; IP Australia Grant Certificate (201710): Canberra, Australia, 2017.
38. Islam, F.R.; Prakash, K.; Mamun, K.A.; Lallu, A.; Pota, H.R. Aromatic Network: A Novel Structure for Power Distribution System. *IEEE Access* **2017**, *5*, 25236–25257. [CrossRef]
39. Yun, Z.; Junjie, L.; Ji, C.; Hua, W. A Framework Research of Power Distribution Equipment Condition Monitoring Cloud Platform Based on RESTful Web Service. In Proceedings of the IEEE Conference on Energy Internet and Energy System Integration (EI2), Beijing, China, 26–28 November 2017; pp. 1–6.
40. Dugan, R. Distribution Test Feeders—Distribution Test Feeder Working Group—IEEE PES Distribution System Analysis Subcommittee. Ewh.ieee.org, 2017. Available online: https://ewh.ieee.org/soc/pes/dsacom/testfeeders/ (accessed on 21 January 2020).
41. Lallu, A.; Islam, F.R.; Mamun, K.A.; Prakash, K.; Cirrincione, M. Power Quality Improvement of Distribution Network Using Optimum Combination of Battery Energy Storage System and capacitor Banks. In Proceedings of the 2017 4th Asia-Pacific World Congress on Computer Science and Engineering (APWC on CSE), Nadi, Fiji, 11–13 December 2017; pp. 193–199.